Supplementary information

Characterization of carbonaceous aerosols in Singapore: insight from black carbon fragments and trace metal ions detected by a soot-particle aerosol mass spectrometer

Laura-Hélèna Rivellini[1], Max G. Adam[2#], Nethmi Kasthuriarachchi[2], Alex. K.Y. Lee[1,2]

[1] NUS Environmental Research Institute, National University of Singapore, 117411, Singapore
[2] Department of Civil and Environmental Engineering, National University of Singapore, 117576, Singapore
[#] Now at Department of Civil and Environmental Engineering, National University of Singapore, 117576, Singapore

Correspondence to: Alex K. Y. Lee (ceelkya@nus.edu.sg)

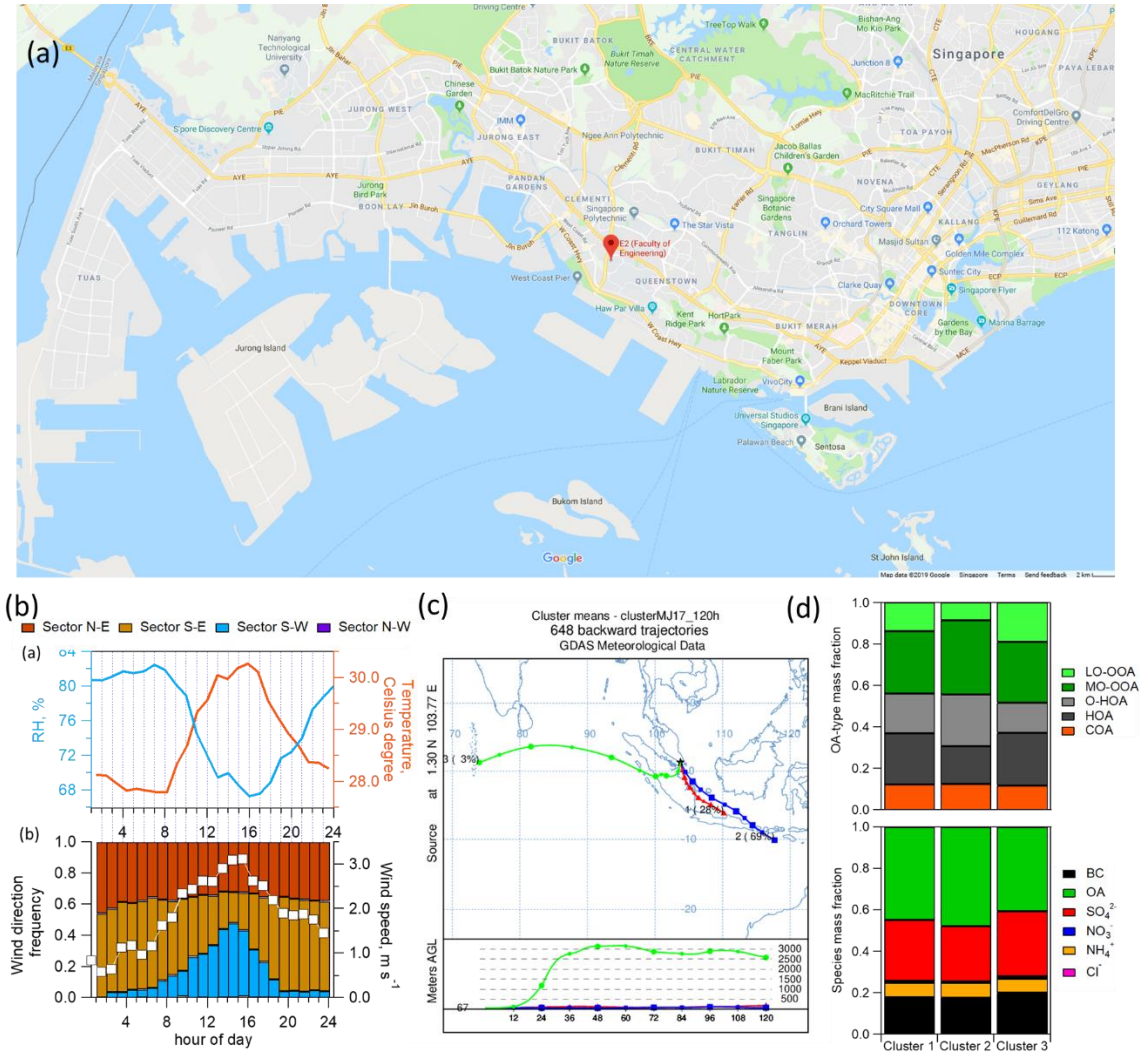

Figure S1: (a) Map overview of the measurement location (indicated by red pin) with industrial areas to the south-west (Tuas industrial estate and Jurong Island). (b) Diurnal cycle of (a) average co-located RH (%) and Temperature (Degree Celsius), (b) wind frequency per sector (N-E: 0-90°; S-E: 90-160°; S-W: 160-270°; N-W: 270-0°) and mean wind speed (m s^{-1}). (c) 3-cluster solution and (d) average composition of PM_1 and OA fraction per cluster. Cluster 1 and 2 back-trajectories originate from the South of East Java and reaching the site by the South to South-East sector after being transported over the Java sea and passing before that over Bali, for Cluster 1, and above Surabaya, for Cluster 2. Cluster 3 originate from Jakarta before passing along the Eastern shore of Sumatra, Indonesia.

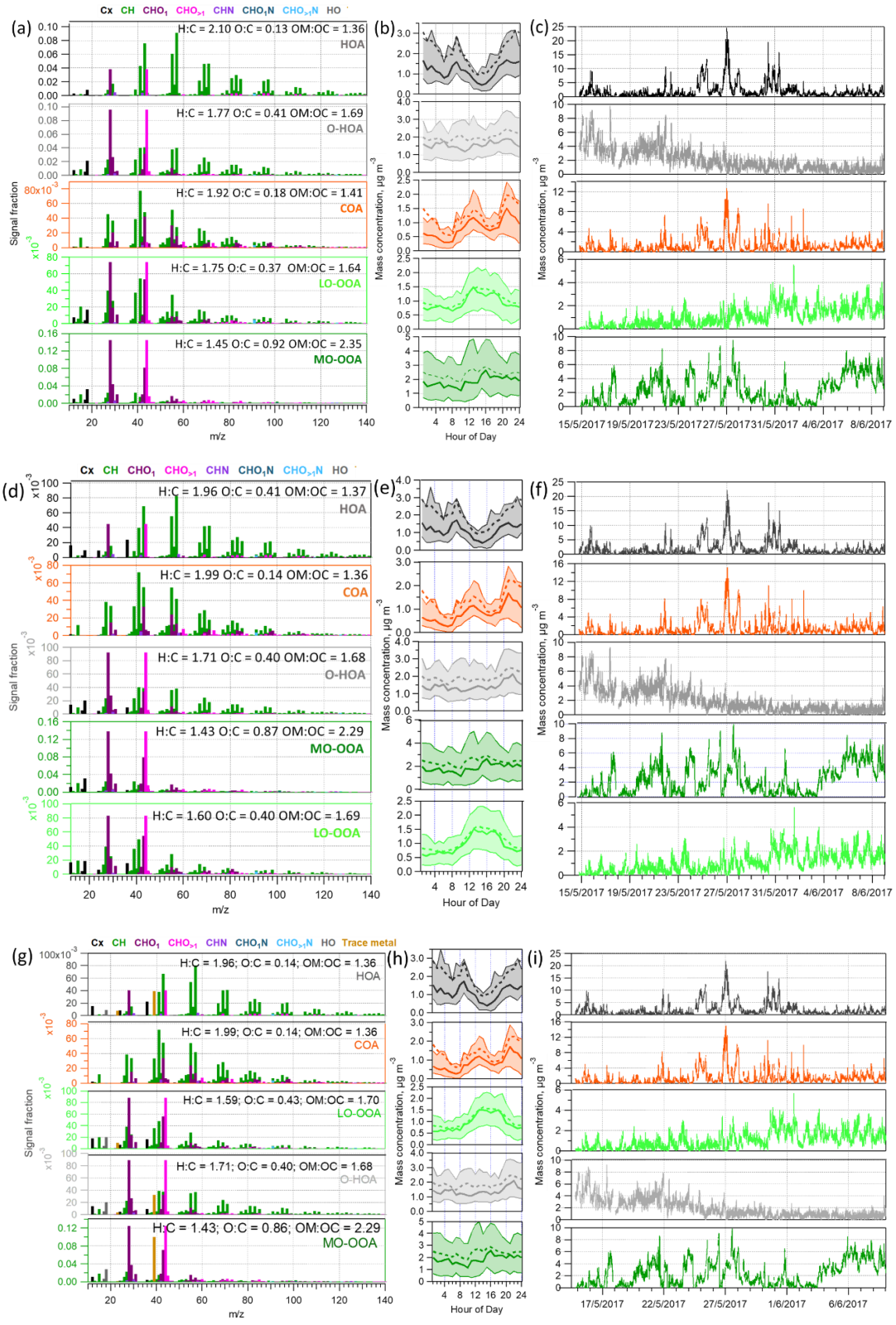

Figure S2: OA component (a,d,g) mass spectrum and elemental ratios, (b,e,h) corresponding diurnal cycles (median - plain line, mean – dotted line, 25th and 75th centiles - shaded area) and (c,f,i) time series for the entire campaign obtained for PMF analysis using laser-on measurements of organics (a,b,c), organics and rBC fragments (C_n^+: C_1^+-C_9^+) (d,e,f) and organics, C_n^+ and metal ions (g,h,i).

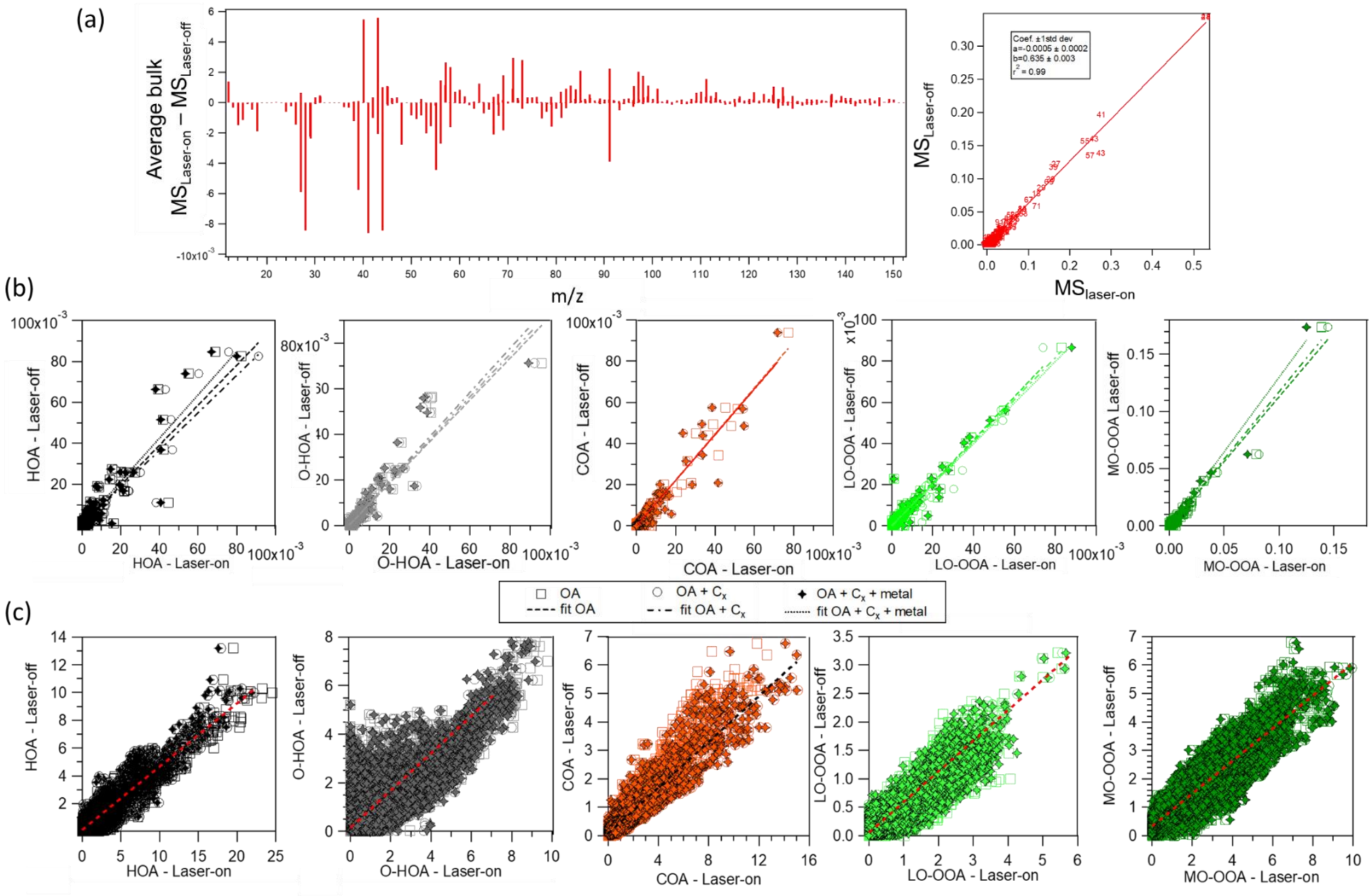

Figure S3: (a) Mass spectral difference (right) and scatter plot (right) of averaged total organics between laser-off and laser-on (including C_n^+) conditions with number indicating m/z fragment. (b) Mass spectra and (c) time series scatter plots of individual OA components obtained from laser-off and laser-on (OA only, including C_n^+ and including C_n^+ and metal) PMF.

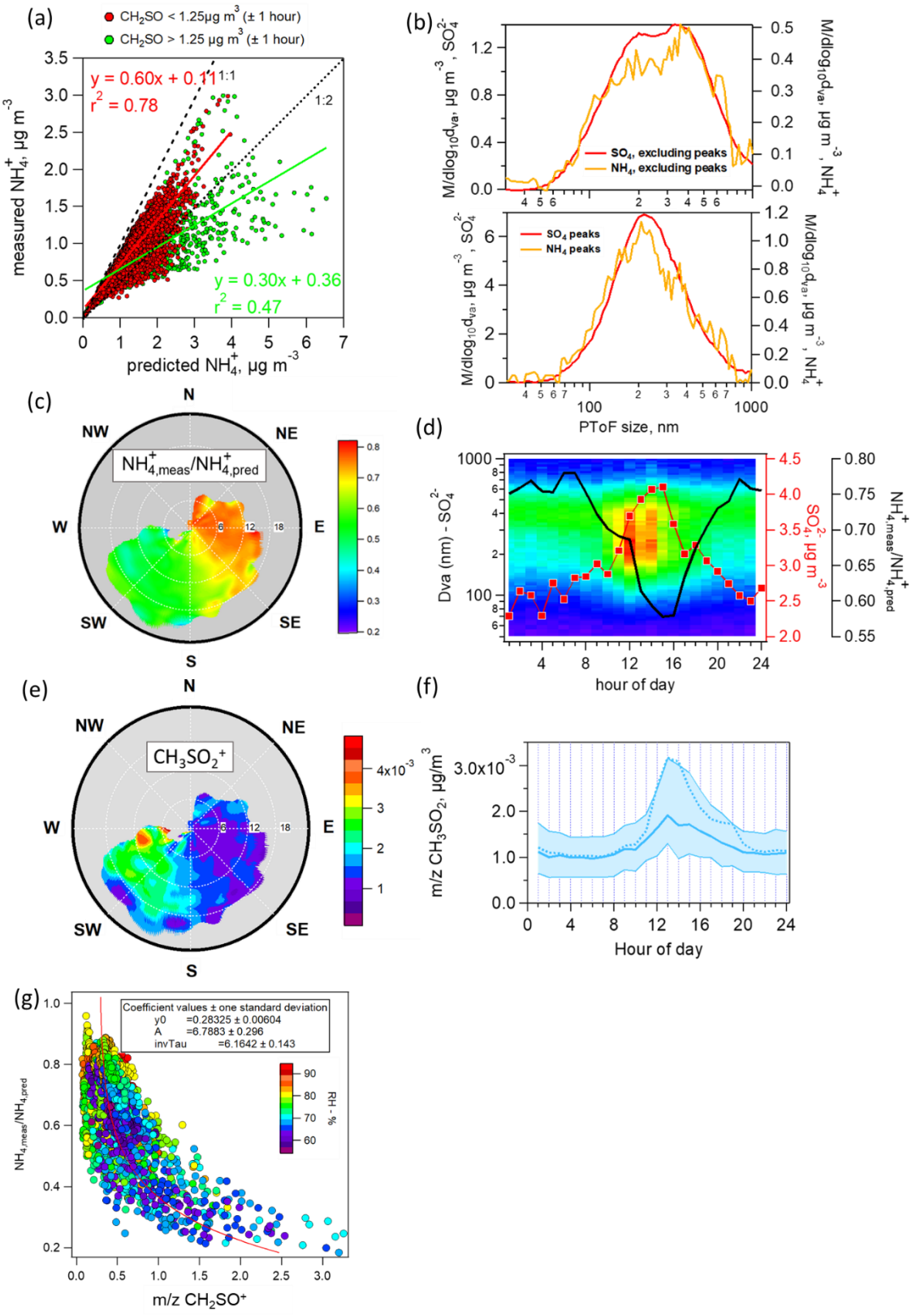

Figure S4: (a) Comparison between measured and predicted NH_4^+ for data originating from South West and other direction, (b) size distributions of SO_4^{2-} and NH_4^+ (top) excluding and (bottom) only considering data excluding SO_4^{2-} concentrations superior to 7 µg m^{-3} of SO_4^{2-}. (c) NWR graph of measured to predicted NH_4^+ and (d) diurnal cycle of SO_4^{2-} size distribution, SO_4 concentrations and measured to predicted NH_4^+ ratio. (e) NWR graph and (f) diurnal cycle of $CH_3SO_2^+$ fragment (median - plain line, mean – dotted line, 25th and 75th centiles - shaded area) and (g) scatter plot of measured to predicted NH_4^+ vs CH_2SO^+ fragment.

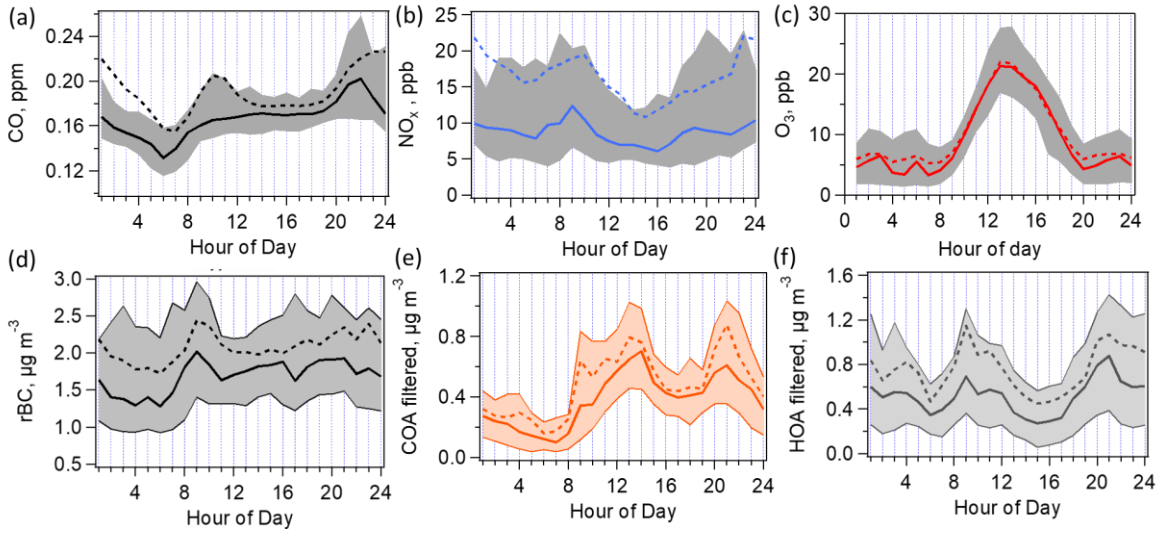

Figure S5: Diurnal cycle of gas-phase species (a) NO_x (b) CO, (c) O_3, and particle phase species (d) rBC, (e) COA and (f) HOA both filtered from 25th to 28th of May, over the campaign. The plain and dotted lines represent, respectively, the medians and averages and the shaded region represents the 25th and 75th percentile.

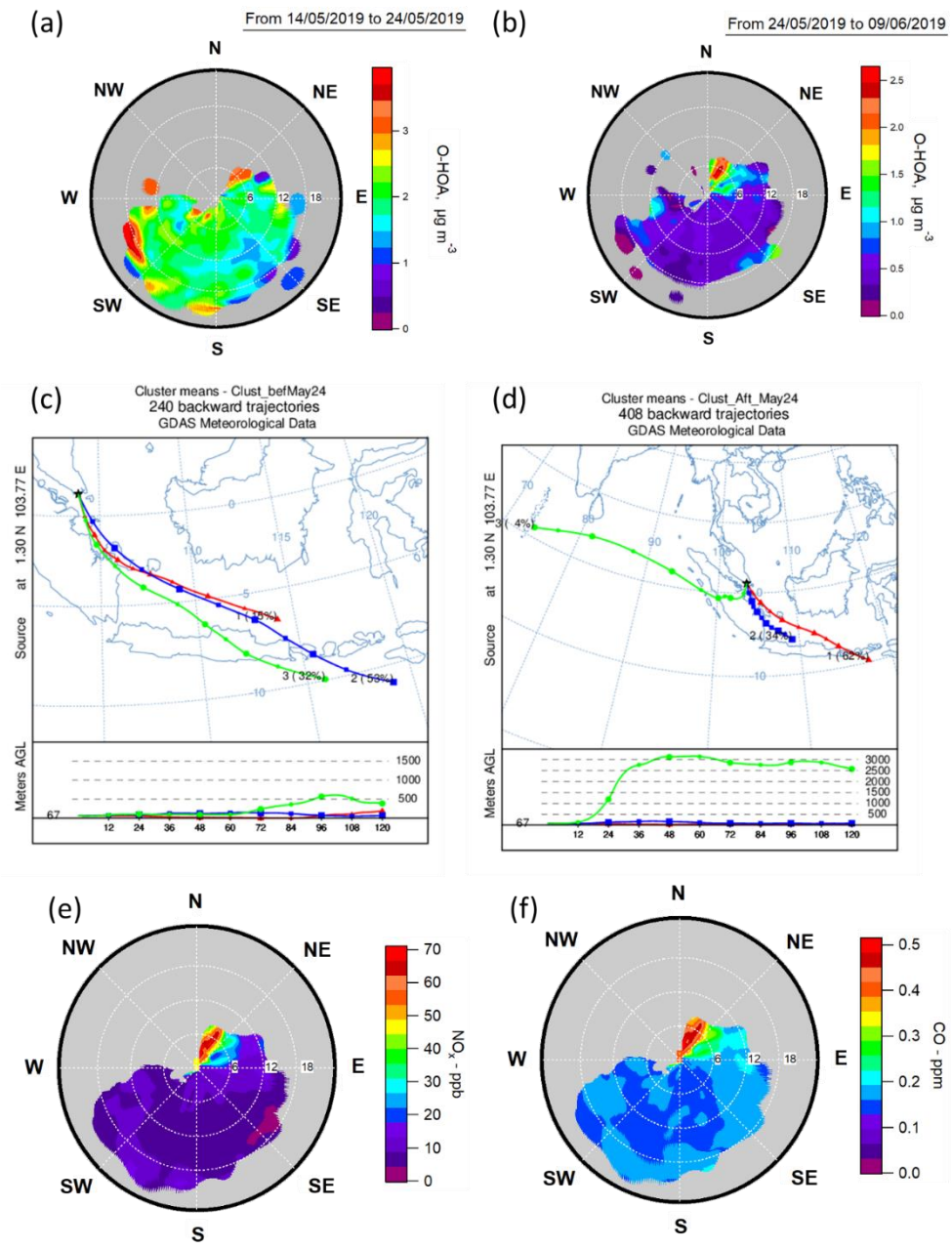

Figure S6: NWR polar graph of O-HOA (a) before and (b) after May 24th 2017 and cluster analysis of 120h back-trajectories for trajectories (c) before and (d) after May 24th 2017, (e) NO_x and (f) CO during the whole period.

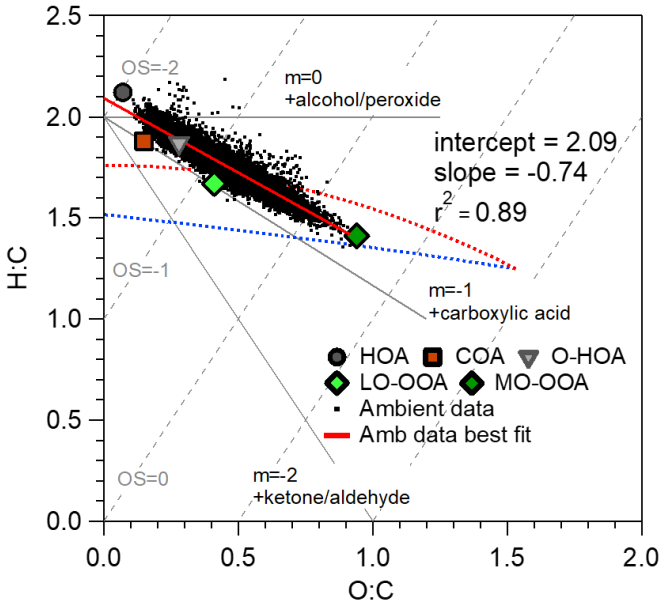

Figure S7: Elemental ratios of ambient data and PMF factors (coloured symbols) determined from the improved-ambient elemental ratio analysis following the method outlined by Canagaratna et al., (2015).

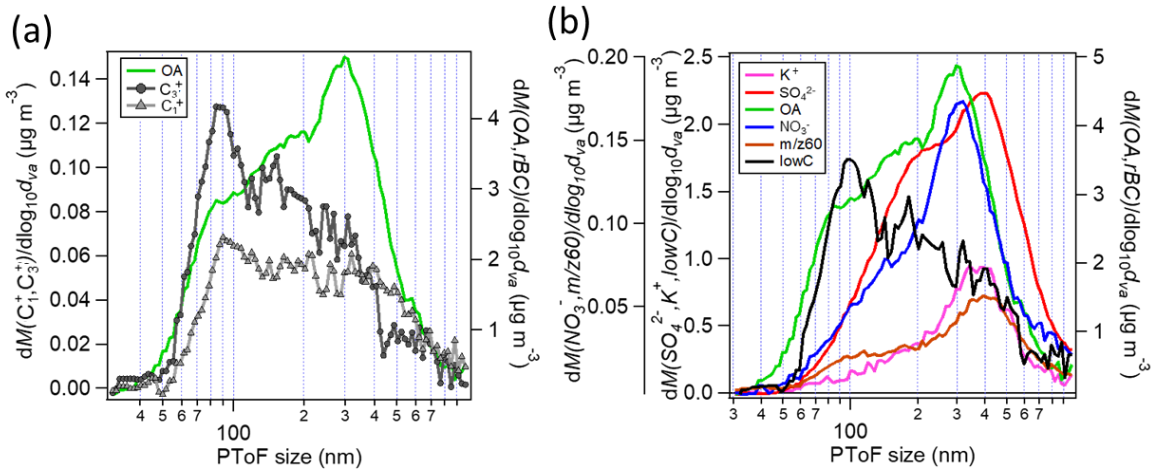

Figure S8: Laser-on average size distributions of (a) m/z 12 (C_1^+), m/z 36 (C_3^+), OA and rBC, and (b) lowC (sum of C_1^+, C_2^+ and C_3^+), NR-PM_1, K^+, Na^+ and m/z 60.

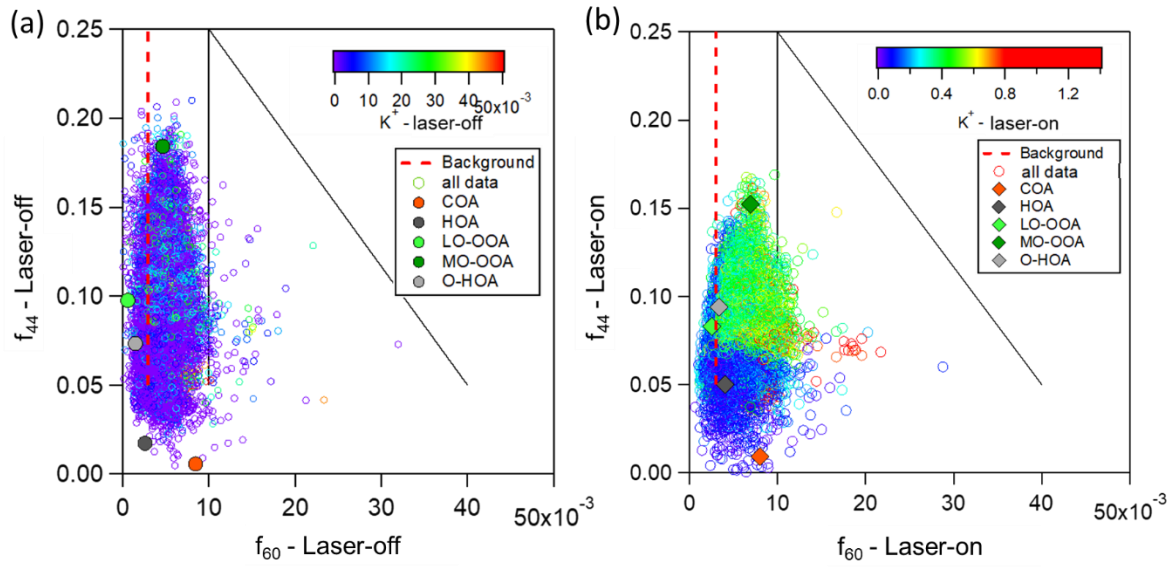

Figure S9: Scatter plots of f_{44} vs f_{60} colored by potassium (K^+) ion signal based on (a) Tungsten vaporizer and (b) dual vaporizers measurements (Dash red line – 0.3% background value, plain lines define the space with (inside the triangular region) and without BB influence (outside the triangular region, Cubison et al. (2011)).

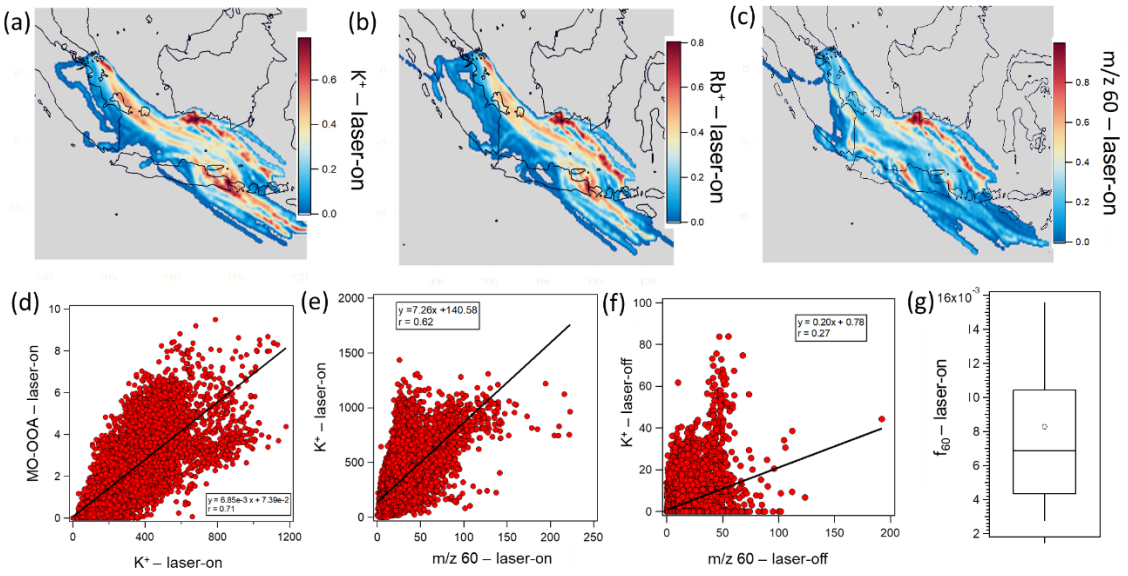

Figure S10: PSCF graphs of dual vaporizer (a) K^+ and (b) Rb^+ and (c) m/z 60. Scatter plots of (d) MO-OOA vs. K^+ signal and (e) K^+ signal vs. m/z 60 for Tungsten vaporizer only and (f) K^+ signal vs. m/z 60 for dual vaporizer mode. (g) Box plots of f_{60} with 5th, 25th, 50th, 75th and 95th percentiles and average value indicated by the marker.

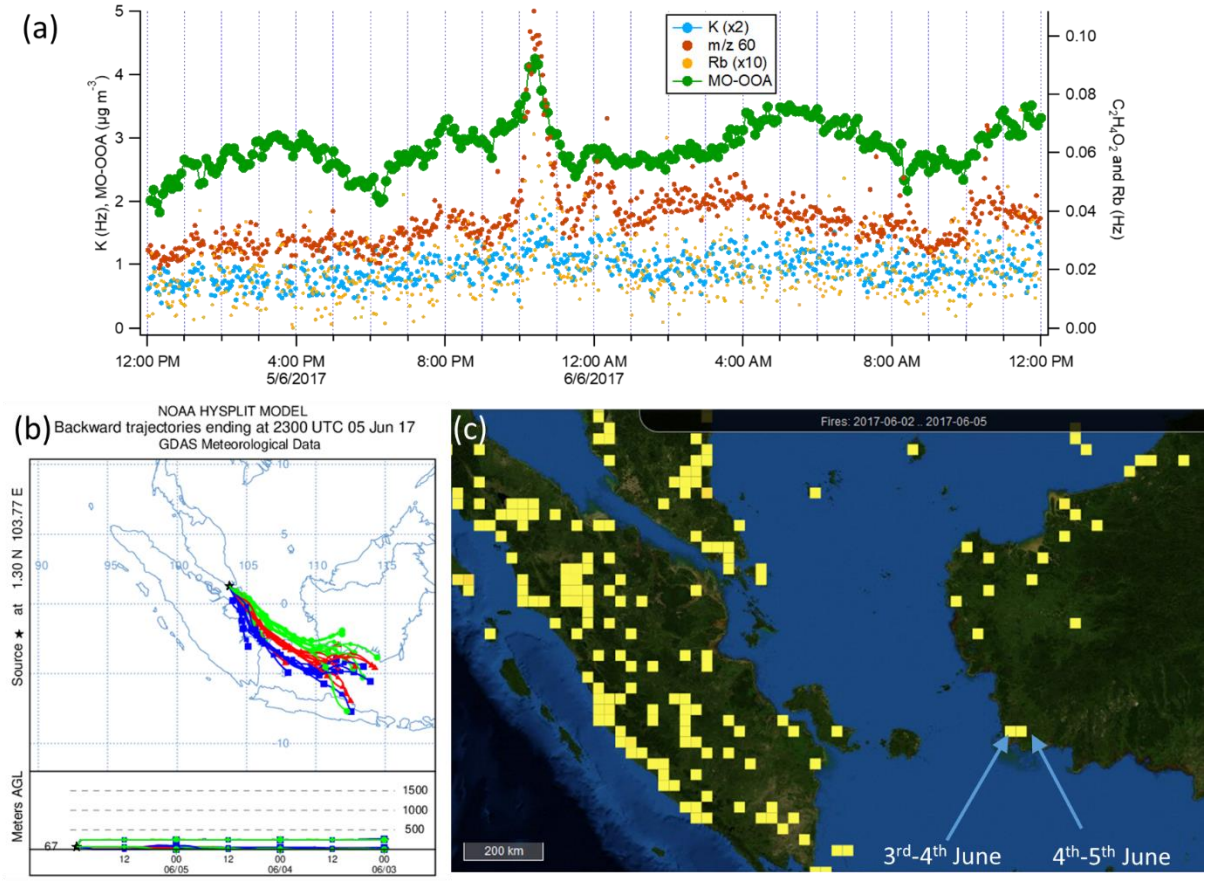

Figure S11: (a) Time series of MO-OOA, m/z 60, K^+ and Rb^+ from June 5th to 6th 2017, (b) 72h back trajectories from June 5th at 23:00 and map of fire occurrences (Modis Active fire products) from June 2nd to 5th 2017.

Table S1: Laser-on trace metal ions signal limit of detection (LOD), average and standard deviation values for the entire period of the campaign. Note that DL was calculated as three time the standard deviation of each ions from filter periods.

Signal (Hz)	K^+	Na^+	Rb^+	V^+	Ni^+
LOD	36.09	22.21	0.82	0.33	0.66
Mean	335.82	31.62	1.29	2.28	0.48
Std Dev.	210.63	24.87	1.05	2.38	0.61

Table S2: Correlation coefficient and slope of linear regression between OA components from laser-off and laser-on including OA only, OA and C_n^+ fragments and OA, C_n^+ fragments and metals ions.

		HOA		COA		O-HOA		LO-OOA		MO-OOA	
		MS	**TS**	**MS**	**TS**	**MS**	**TS**	**MS**	**TS**	**MS**	**TS**
OA	**Slope**	0.98	0.44	1.12	0.50	0.91	0.61	1.05	0.54	1.13	0.62
	R	**0.95**	**0.95**	**0.98**	**0.94**	**0.95**	**0.85**	**0.97**	**0.94**	**0.99**	**0.92**
OA + C_n^+	**Slope**	0.99	0.46	1.11	0.41	0.94	0.59	1.01	0.53	1.17	0.58
	R	**0.91**	**0.92**	**0.95**	**0.92**	**0.95**	**0.80**	**0.98**	**0.92**	**0.99**	**0.91**
OA + C_n^+ + metal	**Slope**	1.06	0.45	1.11	0.40	0.97	0.58	0.99	0.50	1.30	0.58
	R	**0.93**	**0.91**	**0.95**	**0.94**	**0.95**	**0.78**	**0.99**	**0.93**	**0.99**	**0.91**

References

Canagaratna, M. R., Jimenez, J. L., Kroll, J. H., Chen, Q., Kessler, S. H., Massoli, P., Hildebrandt Ruiz, L., Fortner, E., Williams, L. R., Wilson, K. R., Surratt, J. D., Donahue, N. M., Jayne, J. T. and Worsnop, D. R.: Elemental ratio measurements of organic compounds using aerosol mass spectrometry: characterization, improved calibration, and implications, Atmos Chem Phys, 15(1), 253–272, doi:10.5194/acp-15-253-2015, 2015.

Cubison, M. J., Ortega, A. M., Hayes, P. L., Farmer, D. K., Day, D., Lechner, M. J., Brune, W. H., Apel, E., Diskin, G. S., Fisher, J. A., Fuelberg, H. E., Hecobian, A., Knapp, D. J., Mikoviny, T., Riemer, D., Sachse, G. W., Sessions, W., Weber, R. J., Weinheimer, A. J., Wisthaler, A. and Jimenez, J. L.: Effects of aging on organic aerosol from open biomass burning smoke in aircraft and laboratory studies, Atmos Chem Phys, 11(23), 12049–12064, doi:10.5194/acp-11-12049-2011, 2011.